

# Preliminary results on the $^{233}\text{U}$ capture cross section and alpha ratio measured at n\_TOF (CERN) with the fission tagging technique

M. Bacak<sup>1,2,3,\*</sup>, M. Aiche<sup>4</sup>, G. Bélier<sup>5</sup>, E. Berthoumieux<sup>3</sup>, M. Diakaki<sup>3</sup>, E. Dupont<sup>3</sup>, F. Gunsing<sup>3,1</sup>, J. Heyse<sup>6</sup>, S. Kopecky<sup>6</sup>, B. Laurent<sup>5</sup>, H. Leeb<sup>2</sup>, L. Mathieu<sup>4</sup>, P. Schillebeeckx<sup>6</sup>, O. Serot<sup>7</sup>, J. Taieb<sup>5</sup>, V. Vlachoudis<sup>1</sup>, O. Aberle<sup>1</sup>, J. Andrzejewski<sup>8</sup>, L. Audouin<sup>9</sup>, J. Balibrea<sup>10</sup>, M. Barbagallo<sup>11</sup>, F. Bečvář<sup>12</sup>, J. Billowes<sup>13</sup>, D. Bosnar<sup>14</sup>, A. Brown<sup>15</sup>, M. Caamaño<sup>16</sup>, F. Calviño<sup>17</sup>, M. Calviani<sup>1</sup>, D. Cano-Ott<sup>10</sup>, R. Cardella<sup>1</sup>, A. Casanovas<sup>17</sup>, F. Cerutti<sup>1</sup>, Y. H. Chen<sup>9</sup>, E. Chiaveri<sup>1,13,18</sup>, N. Colonna<sup>11</sup>, G. Cortés<sup>17</sup>, M. A. Cortés-Giraldo<sup>18</sup>, L. Cosentino<sup>19</sup>, L. A. Damone<sup>11,20</sup>, C. Domingo-Pardo<sup>21</sup>, R. Dressler<sup>22</sup>, I. Durán<sup>16</sup>, B. Fernández-Domínguez<sup>16</sup>, A. Ferrari<sup>1</sup>, P. Ferreira<sup>23</sup>, P. Finocchiaro<sup>19</sup>, V. Furman<sup>24</sup>, K. Göbel<sup>25</sup>, A. R. García<sup>10</sup>, A. Gawlik<sup>8</sup>, S. Gilardoni<sup>1</sup>, T. Glodariu<sup>†26</sup>, I. F. Gonçalves<sup>23</sup>, E. González-Romero<sup>10</sup>, E. Griesmayer<sup>2</sup>, C. Guerrero<sup>18</sup>, H. Harada<sup>27</sup>, S. Heinitz<sup>22</sup>, D. G. Jenkins<sup>15</sup>, E. Jericha<sup>2</sup>, F. Käppeler<sup>28</sup>, Y. Kadi<sup>1</sup>, A. Kalamara<sup>29</sup>, P. Kavargin<sup>2</sup>, A. Kimura<sup>27</sup>, N. Kivel<sup>22</sup>, I. Knapova<sup>12</sup>, M. Kokkoris<sup>29</sup>, M. Krtička<sup>12</sup>, D. Kurtulgil<sup>25</sup>, E. Leal-Cidoncha<sup>16</sup>, C. Lederer<sup>30</sup>, J. Lerendegui-Marco<sup>18</sup>, S. Lo Meo<sup>31,32</sup>, S. J. Lonsdale<sup>30</sup>, D. Macina<sup>1</sup>, A. Manna<sup>32,33</sup>, J. Marganec<sup>8,34</sup>, T. Martínez<sup>10</sup>, A. Masi<sup>1</sup>, C. Massimi<sup>32,33</sup>, P. Mastinu<sup>35</sup>, M. Mastromarco<sup>11</sup>, E. A. Mauger<sup>22</sup>, A. Mazzone<sup>11,36</sup>, E. Mendoza<sup>10</sup>, A. Mengoni<sup>31</sup>, P. M. Milazzo<sup>37</sup>, F. Mingrone<sup>1</sup>, A. Musumarra<sup>19,38</sup>, A. Negret<sup>26</sup>, R. Nolte<sup>34</sup>, A. Oprea<sup>26</sup>, N. Patronis<sup>39</sup>, A. Pavlik<sup>40</sup>, J. Perkowski<sup>8</sup>, I. Porras<sup>41</sup>, J. Praena<sup>41</sup>, J. M. Quesada<sup>18</sup>, D. Radeck<sup>34</sup>, T. Rauscher<sup>42,43</sup>, R. Reifarth<sup>25</sup>, C. Rubbia<sup>1</sup>, J. A. Ryan<sup>13</sup>, M. Sabaté-Gilarte<sup>1,18</sup>, A. Saxena<sup>44</sup>, D. Schumann<sup>22</sup>, P. Sedyshev<sup>24</sup>, A. G. Smith<sup>13</sup>, N. V. Sosnin<sup>13</sup>, A. Stamatopoulos<sup>29</sup>, G. Tagliente<sup>11</sup>, J. L. Tain<sup>21</sup>, A. Tarifeño-Saldivia<sup>17</sup>, L. Tassan-Got<sup>9</sup>, S. Valenta<sup>12</sup>, G. Vannini<sup>32,33</sup>, V. Variale<sup>11</sup>, P. Vaz<sup>23</sup>, A. Ventura<sup>32</sup>, R. Vlastou<sup>29</sup>, A. Wallner<sup>45</sup>, S. Warren<sup>13</sup>, C. Weiss<sup>2</sup>, P. J. Woods<sup>30</sup>, T. Wright<sup>13</sup>, P. Žugec<sup>14,1</sup>

<sup>1</sup>European Organization for Nuclear Research (CERN), Switzerland

<sup>2</sup>Technische Universität Wien, Austria

<sup>3</sup>CEA Irfu, Université Paris-Saclay, F-91191 Gif-sur-Yvette, France

<sup>4</sup>CENBG, CNRS/IN2P3-Université de Bordeaux, Gradignan, France

<sup>5</sup>CEA, DAM, DIF, F-91297 Arpajon, France

<sup>6</sup>European Commission, Joint Research Centre, Geel, Retieseweg 111, B-2440 Geel, Belgium

<sup>7</sup>CEA, DEN, Cadarache, France

<sup>8</sup>University of Lodz, Poland

<sup>9</sup>Institut de Physique Nucléaire, CNRS-IN2P3, Univ. Paris-Sud, Université Paris-Saclay, F-91406 Orsay Cedex, France

<sup>10</sup>Centro de Investigaciones Energéticas Medioambientales y Tecnológicas (CIEMAT), Spain

<sup>11</sup>Istituto Nazionale di Fisica Nucleare, Sezione di Bari, Italy

<sup>12</sup>Charles University, Prague, Czech Republic

<sup>13</sup>University of Manchester, United Kingdom

<sup>14</sup>Department of Physics, Faculty of Science, University of Zagreb, Zagreb, Croatia

<sup>15</sup>University of York, United Kingdom

\*corresponding author: michael.bacak@cern.ch

- <sup>16</sup>University of Santiago de Compostela, Spain  
<sup>17</sup>Universitat Politècnica de Catalunya, Spain  
<sup>18</sup>Universidad de Sevilla, Spain  
<sup>19</sup>INFN Laboratori Nazionali del Sud, Catania, Italy  
<sup>20</sup>Dipartimento di Fisica, Università degli Studi di Bari, Italy  
<sup>21</sup>Instituto de Física Corpuscular, CSIC - Universidad de Valencia, Spain  
<sup>22</sup>Paul Scherrer Institut (PSI), Villingen, Switzerland  
<sup>23</sup>Instituto Superior Técnico, Lisbon, Portugal  
<sup>24</sup>Joint Institute for Nuclear Research (JINR), Dubna, Russia  
<sup>25</sup>Goethe University Frankfurt, Germany  
<sup>26</sup>Horia Hulubei National Institute of Physics and Nuclear Engineering, Romania  
<sup>27</sup>Japan Atomic Energy Agency (JAEA), Tokai-mura, Japan  
<sup>28</sup>Karlsruhe Institute of Technology, Campus North, IKP, 76021 Karlsruhe, Germany  
<sup>29</sup>National Technical University of Athens, Greece  
<sup>30</sup>School of Physics and Astronomy, University of Edinburgh, United Kingdom  
<sup>31</sup>Agenzia nazionale per le nuove tecnologie (ENEA), Bologna, Italy  
<sup>32</sup>Istituto Nazionale di Fisica Nucleare, Sezione di Bologna, Italy  
<sup>33</sup>Dipartimento di Fisica e Astronomia, Università di Bologna, Italy  
<sup>34</sup>Physikalisch-Technische Bundesanstalt (PTB), Bundesallee 100, 38116 Braunschweig, Germany  
<sup>35</sup>Istituto Nazionale di Fisica Nucleare, Sezione di Legnaro, Italy  
<sup>36</sup>Consiglio Nazionale delle Ricerche, Bari, Italy  
<sup>37</sup>Istituto Nazionale di Fisica Nucleare, Sezione di Trieste, Italy  
<sup>38</sup>Dipartimento di Fisica e Astronomia, Università di Catania, Italy  
<sup>39</sup>University of Ioannina, Greece  
<sup>40</sup>University of Vienna, Faculty of Physics, Vienna, Austria  
<sup>41</sup>University of Granada, Spain  
<sup>42</sup>Department of Physics, University of Basel, Switzerland  
<sup>43</sup>Centre for Astrophysics Research, University of Hertfordshire, United Kingdom  
<sup>44</sup>Bhabha Atomic Research Centre (BARC), India  
<sup>45</sup>Australian National University, Canberra, Australia

**Abstract.**  $^{233}\text{U}$  is of key importance among the fissile nuclei in the Th-U fuel cycle. A particularity of  $^{233}\text{U}$  is its small neutron capture cross-section, which is on average about one order of magnitude lower than the fission cross-section. The accuracy in the measurement of the  $^{233}\text{U}$  capture cross-section depends crucially on an efficient capture-fission discrimination, thus a combined set-up of fission and  $\gamma$ -detectors is needed. A measurement of the  $^{233}\text{U}$  capture cross-section and capture-to-fission ratio was performed at the CERN n\_TOF facility. The Total Absorption Calorimeter (TAC) of n\_TOF was employed as  $\gamma$ -detector coupled with a novel compact ionization chamber as fission detector. A brief description of the experimental set-up will be given, and essential parts of the analysis procedure as well as the preliminary response of the set-up to capture are presented and discussed.

## 1 Introduction

The Th-U fuel cycle [1,2] has been proposed as an alternative to the U-Pu fuel cycle for nuclear power. As one of the key nuclei,  $^{233}\text{U}$  influences many parts of the design of a nuclear power plant like neutronics performance, economics, nuclear safety, etc. The available data for the  $^{233}\text{U}$  capture cross section are scarce, as shown in Fig. 1, because the measurement is challenging due to the competing fission reaction which is on average one order of magnitude more likely than the capture cross section, see Fig. 2. The first measurement [3] at the n\_TOF facility [4] at CERN was successfully performed but proved to be challenging due to the need

to accurately distinguish between capture and fission  $\gamma$ -rays without any additional discrimination tool.

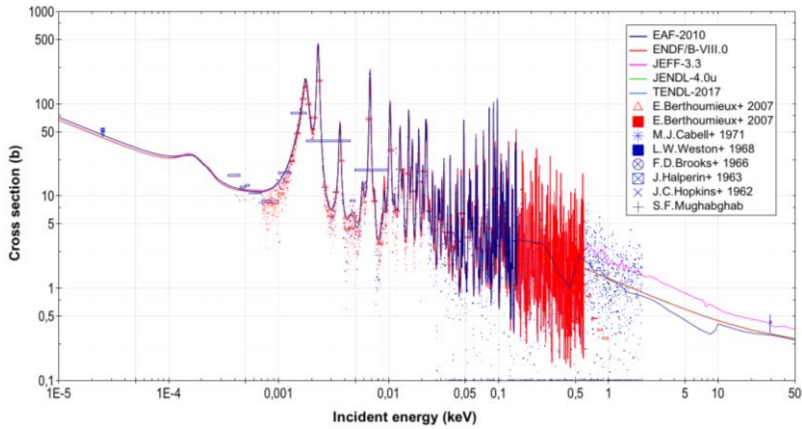


**Fig. 1.** Existing data sets and evaluations for the  $^{233}\text{U}$  capture cross section.

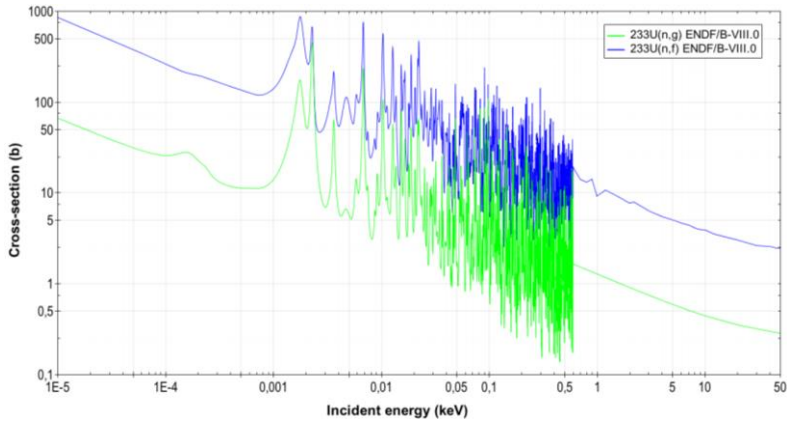


**Fig. 2.**  $^{233}\text{U}$  fission and capture cross section in comparison.

A new measurement [5] was proposed at  $n\_TOF$  and performed at the end of 2016, aiming to provide a higher level of discrimination between the competing capture and fission channels and to obtain more precise and accurate data up to 10 keV neutron energy. As the accuracy in the measurement of the  $^{233}\text{U}$  capture cross-section essentially relies on an efficient capture-fission discrimination, a combined set-up of  $\gamma$ -detectors and fission detectors was used, described in sections 2.3 and 2.4, respectively. A similar methodology of extracting the capture cross-section of fissile actinides has been under development at the DANCE facility at the Los Alamos National Laboratory [6,7].

## 2 Experimental Setup

### 2.1 The $n\_TOF$ facility

At the  $n\_TOF$  facility neutrons are produced by spallation reactions of 20 GeV/c protons provided by CERN's Proton Synchrotron impinging on a lead target. The target is surrounded by water acting as a coolant and moderator for the initially fast neutron spectrum resulting in a white neutron beam with neutron energies ranging from sub-thermal up to GeV, see Fig. 3.

The high intensity pulsed proton beam with a maximum frequency of 0.83 Hz results in a high instantaneous neutron flux in the experimental area. The measurement was performed at the experimental area 1 (EAR1), located at 185 m from the neutron-producing target. The neutron beam intensity in EAR1 is constantly monitored with four out-of-beam silicon detectors (*SiMon*) [8] measuring the outgoing particles of the standard reaction  ${}^6\text{Li}(n,t)$  reaction from a  $600\ \mu\text{m}/\text{cm}^2$  thick  ${}^6\text{Li}$  foil intersecting the beam.

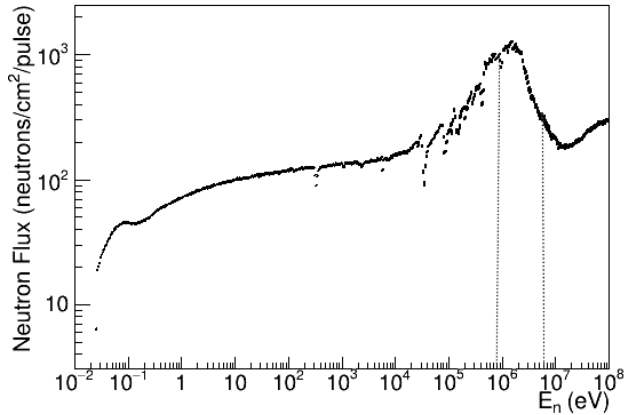


**Fig. 3.** Neutron Flux at  $n_{\text{-TOF}}$  EAR1. The dashed lines indicate the region of  $800\ \text{keV} < E_n < 7\ \text{MeV}$  corresponding to  $5\ \mu\text{s} < \text{TOF} < 15\ \mu\text{s}$  (see discussion in section 3.1).

## 2.2 ${}^{233}\text{U}$ targets

The  ${}^{233}\text{U}$  deposits for the measurement have been prepared by JRC-Geel by molecular plating. The base material was 99.936 % enriched in  ${}^{233}\text{U}$  with the largest contaminant being 0.0496 %  ${}^{234}\text{U}$  (Lot 2146, TP2015-10). Samples 4 cm in diameter covering the full neutron beam were deposited on  $10\ \mu\text{m}$  thick aluminium backings. A total mass of 46.5 mg  ${}^{233}\text{U}$  was distributed over 14 samples with an average areal density of about  $250\ \mu\text{g}/\text{cm}^2$  and an average activity of about 1 MBq per sample.

## 2.3 Gamma-Detector

The Total Absorption Calorimeter (TAC) [9] is designed as a high efficiency calorimeter to detect the complete prompt  $\gamma$ -ray cascade emitted in nuclear reactions. It consists of 40  $\text{BaF}_2$  crystals forming a hollow sphere with an inner radius of 10.6 cm covering almost  $4\pi$  solid angle minus two opposite channels which are left open for entrance and exit of the neutron beam, see Fig. 4. The fission detector was placed at the centre of the TAC surrounded by the so-called *absorber*, a spherical neutron shielding aiming to reduce the background introduced by scattered neutrons into the crystals. The absorber is made out of polyethylene and 7.5 % natural lithium salt.

The digitised waveforms are analysed offline with a dedicated pulse shape analysis routine [10], and the individual signals are grouped together in events by setting an adequate coincidence window of 12 ns between signals. Each of those events is characterised by its time-of-flight  $\text{TOF}$ , determining the neutron energy  $E_n$ , the total deposited energy in the TAC  $E_{\text{Sum}}$ , and the number of hit crystals  $m_{\text{cr}}$ . One of the main advantages of the TAC is the use of the quantities  $m_{\text{cr}}$  and  $E_{\text{Sum}}$  to discriminate between different types of reactions. For example, background events from the sample activity or ambient background usually deposit a few MeV of energy in the TAC and are characterised by small crystal multiplicities. On the other

hand, electromagnetic cascades from neutron capture events will deposit energies up to the neutron separation energy of the compound nucleus with larger average multiplicities. Hence, selecting the right subset of events with respect to  $m_{cr}$  and  $E_{Sum}$  will result in an improved capture-to-background ratio.

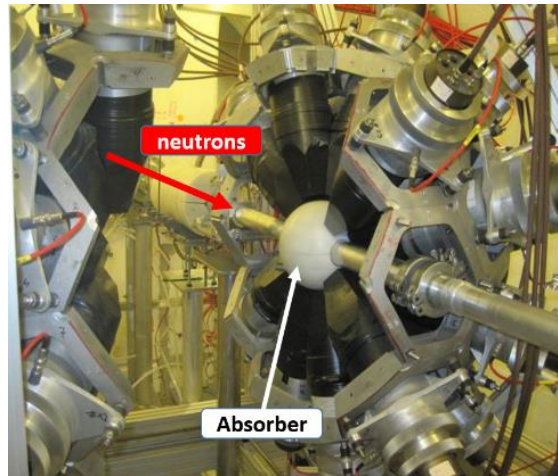


**Fig. 4.** The n\_TOF Total Absorption Calorimeter.

## 2.4 Fission Detector

A previous experiment [11] at n\_TOF using MicroMegas (MGAS) detectors as fission detector showed that the copper mesh of the MicroMegas is a significant source of background for neutron energies above 100 eV. Thus, a novel fission detector was designed, see Fig. 5, respecting the main constraints namely a) the restricted space inside the absorber of the TAC (maximum diameter of 10 cm); b) the fast response needed to reduce pile-up due to the high  $\alpha$ -activity of the  $^{233}\text{U}$  targets; c) the hosting of the maximum number of  $^{233}\text{U}$  targets possible for sufficient statistics in a reasonable beam time. The housing of the fission chamber *FICH* is made of 1.5 mm thick aluminium with an outer diameter of 66 mm and a length of 78 mm. Two stacks of simple axial ionization cells are mounted directly on their respective motherboards and are inserted from each end of the chamber. The 3 mm inter-electrode gap in each cell is biased with 420 V and filled with the fast ionizing gas  $\text{CF}_4$ . Pre-amplifier and shaper modules are directly mounted on the motherboards of each stack to reduce signal attenuation and to improve the signal to noise ratio.

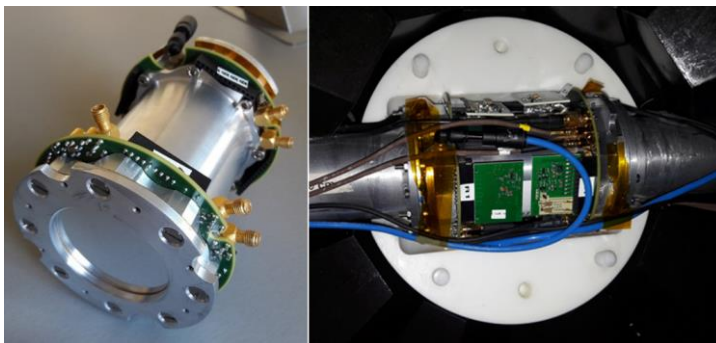


**Fig. 5.** The fission chamber: prototype in the lab (left panel); fully operational chamber mounted inside the white absorber in the TAC (right panel).

### 3 Performance of the FICH

#### 3.1 Discrimination between fission and alpha activity

Fig. 6 shows the performance of the chamber in terms of separation between fission fragments (FF) and  $\alpha$ -particles for various conditions on TOF, hence  $E_n$ . Looking at the full neutron energy range of interest the separation is limited due to the poor FF/ $\alpha$ -ratio. This ratio is drastically improved in resonances of the fission cross section, for example in the energy range  $1.6 \text{ eV} < E_n < 1.9 \text{ eV}$ , corresponding to the first large resonance dominated by fission. The ratio can be further improved when exploiting the shape of the neutron flux at n\_TOF, namely the region between  $800 \text{ keV} < E_n < 7 \text{ MeV}$  or  $5 \mu\text{s} < \text{TOF} < 15 \mu\text{s}$  respectively. In this region the neutron flux has a maximum, see Fig. 3, further improving the fission rate, hence the FF/ $\alpha$ -ratio.

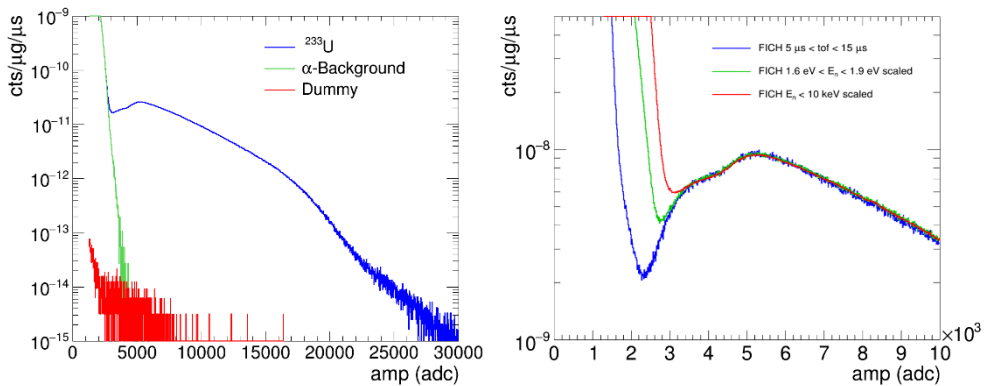


**Fig. 6.** Amplitude spectra of the fission chamber: various contributions for  $0.02 \text{ eV} < E_n < 10 \text{ keV}$  (left panel);  $\alpha$ -FF separation for various conditions on  $E_n$  or TOF (right panel).

#### 3.2 Fission Tagging

The purpose of the fission chamber is to allow identification of the TAC response to fission events by looking at coincidences between FICH and TAC. In Fig. 7 the comparison between the amplitude spectra of the FICH without and with coincidence (tagged) is shown. The tagged spectrum follows the fission fragment shape perfectly even below amplitudes of 3000 channels of the ADC where the main contribution is from  $\alpha$ -particles. In the top left panel of Fig. 8 the response of the TAC to fission events is shown.

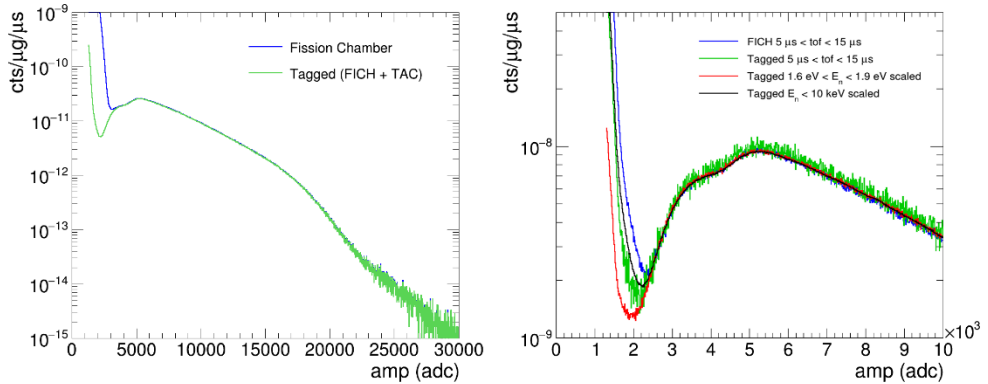


**Fig. 7.** Comparison of the amplitude spectra of the FICH and tagged counts: for  $20 \text{ meV} < E_n < 10 \text{ keV}$  (left panel),  $\alpha$ -FF separation for various conditions on  $E_n$  or TOF (right panel).

## 4 TAC response

### 4.1 Sources of Background

In Fig. 8 the contributions to the total measured spectrum are shown separately. It can be seen that the background consists mostly of low energy events with  $E_{Sum} < 3 \text{ MeV}$  and  $m_{cr} < 3$ . The  $\gamma$ -rays from fission are the main source of background in the region of interest for the capture measurement, i.e. from  $3 \text{ MeV} < E_{Sum} < 7.5 \text{ MeV}$  ( $S_n(^{234}\text{U}) = 6.84 \text{ MeV}$ ). Thus, a precise subtraction of this component is crucial to minimise the uncertainty in the capture cross section.

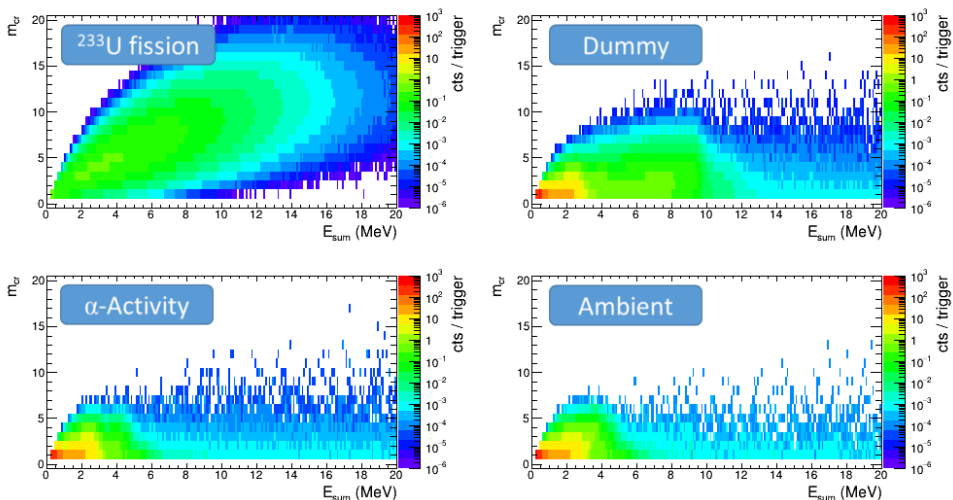


**Fig. 8.** TAC response for various background contributions.

### 4.2 FICH efficiency

The efficiency of the fission detector can be determined under the assumption that mostly fission events deposit energies higher than 10 MeV in the TAC. With the extra assumption

that a fission event is detected independently by the TAC and the FICH the tagging efficiency  $\varepsilon_{\text{Tagg}}$  equals the fission chamber efficiency  $\varepsilon_{\text{FICH}}$

$$\varepsilon_{\text{Tagg}} = \frac{c_{\text{Tagg}}}{c_{\text{TAC}}} = \varepsilon_{\text{FICH}} \quad (1)$$

with  $c_{\text{Tagg}}$  and  $c_{\text{TAC}}$  the tagged and total TAC counts respectively with  $10 < E_{\text{Sum}} < 20$  MeV. The removal of the background contributions can be further improved by gating on high crystal multiplicities. The calculated fission chamber efficiency for fission amplitudes bigger than 3000 channels of the ADC is shown in Fig. 8 for various neutron energy regions. It can be seen that the data points are in a good agreement with a constant value of  $0.867 \pm 0.002$ , see fitted red line in Fig. 9.

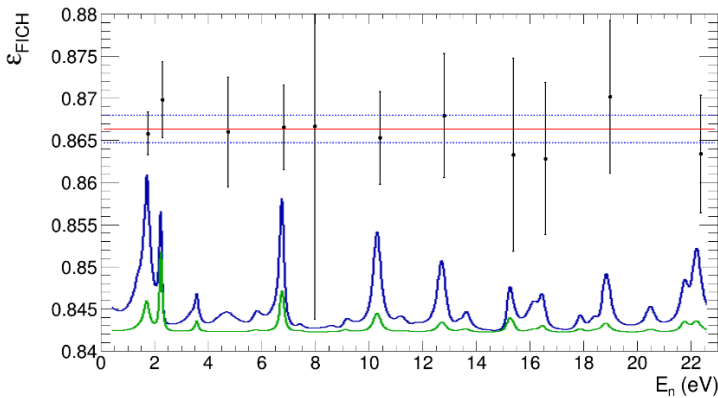


**Fig. 9.** Efficiency of the fission chamber as a function of neutron energy for events with fission amplitudes bigger than 3000 channels of the ADC and  $10 \text{ MeV} < E_{\text{Sum}} < 20 \text{ MeV}$  and  $m_{cr} > 6$ . The red line is a fitted constant function and the blue dashed line indicates the error band of the fit. The solid blue and green line at the bottom illustrate the shape of the ENDF/B-VIII.0 fission and capture cross section respectively.

### 4.3 Response to Capture

In Fig. 10 the total measured deposited energy spectrum compared to the various contributions can be seen in the case of neutrons absorbed in the large capture resonance at  $2.1 \text{ eV} < E_n < 2.5 \text{ eV}$ . The lower cut-off is defined by the 200 keV threshold set per individual detector and a minimum measured multiplicity  $m_{cr} > 2$ . It is evident that the largest contribution are the fission events in the region of interest. The peak in the capture response at the neutron separation energy  $S_n(^{234}\text{U}) = 6.84 \text{ MeV}$  is clearly visible and followed by a smooth bump towards lower energies. Below 2.5 MeV the background subtraction has to be investigated further, because a smooth shape going to zero is expected in the capture response. Above 7.5 MeV there is still some remaining background possibly due to capture of scattered neutrons in the TAC.



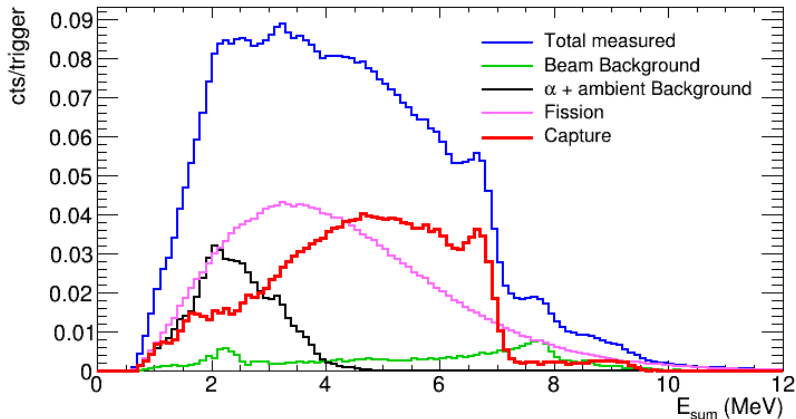


**Fig. 10.** Contributions to the deposited energy spectra in the TAC in the capture resonance at  $2.1 \text{ eV} < E_n < 2.5 \text{ eV}$  for  $2 < m_{cr} < 7$ .

## 5 Summary & Conclusion

The experiment aiming to measure the  $^{233}\text{U}$  capture cross section has been performed successfully at the n\_TOF facility (CERN) using the Total Absorption Calorimeter for the detection of the  $\gamma$ -rays. A fission detector was used in veto to properly remove the contribution from the fission  $\gamma$ -rays. Preliminary analysis of capture results have been presented and are promising.

Two background contributions, namely the scattered neutrons by the  $^{233}\text{U}$  layers and the response of the experimental set-up to fission neutrons are still under investigation. In the next step extensive Monte Carlo simulations will be used to calculate the detection efficiency for the applied analysis cuts regarding deposited energy and crystal multiplicity. For this purpose, the capture cascades will be generated with DICEBOX [12] and fed into Geant4 where the full detector geometry has been reproduced. Furthermore, dead time corrections and pile-up effects [13, 14] will be taken into account.

## References

1. V.G. Pronyaev, IAEA Report, INDC (NDS) **408** (1999)
2. The Generation IV International Forum, <http://www.gen-4.org/> (2013)
3. C. Carrapico et al., Nucl. Instr. Meth. A **704**, 60 (2013)
4. C. Guerrero, and the n\_TOF collaboration, Eur. Phys. J. A **48**, 29 (2012).
5. C. Carrapico, E. Berthoumieux and the n\_TOF Collaboration, CERN-INTC-2013-041 / INTC-P-397 (2013)
6. M. Jandel et al., Phys. Rev. Lett. **109**, 202506 (2012)
7. S. Mosby et al., Phys. Rev. C **89**, 034610 (2014)
8. S. Marrone, et al., Nucl. Instr. and Meth. A **517**, 389 (2004)
9. C. Guerrero and the n\_TOF Collaboration, Nucl. Instr. Meth. A **608**, 424 (2009)
10. E. Berthoumieux, Preliminary report on BaF<sub>2</sub> Total Absorption Calorimeter test measurement, Rap. Tech., CEA-Saclay/DAPNIA/SPhN, (2004)
11. J. Balibrea and the n\_TOF Collaboration, Nuclear Data Sheets, **119**: 10 (2014)
12. F. Bečvář, Nucl Instr Meth A. **417**, 434 (1998)
13. E. Mendoza, et al., Nucl. Instr. and Meth. A **768**, 55 (2014)
14. C. Guerrero, et al., Nucl. Instr. and Meth. A **777**, 63 (2015)